

Single-Molecule Magnets: A Reductive Aggregation Route to New Types of Mn₁₂ Complexes

Philippa King,[†] Wolfgang Wernsdorfer,[‡] Khalil A. Abboud,[†] and George Christou*,[†]

Department of Chemistry, University of Florida, Gainesville, Florida 32611-7200, and Laboratoire Louis Néel-CNRS, BP 166, 25 Avenue des Martyrs, 38042 Grenoble, Cedex 9, France

Received July 11, 2005

Three dodecanuclear Mn clusters [Mn₁₂O₁₀(OMe)₃(OH)(O₂CC₆H₃F₂)₁₆(MeOH)₂]·8MeOH (**1**), [Mn₁₂O₁₀(OMe)₄(O₂-CBu^t)₁₆(MeOH)₂] (**2**), and [Mn₁₂O₁₂(O₂CBu^t)₁₆(MeOH)₄] (**3**) synthesized by reductive aggregation reactions are reported. Clusters **1** and **2** possess a central alkoxide-bridged planar Mn₄ topology, whereas **3** is a new high-symmetry member of the normal Mn₁₂ family. Complexes **1** and **2** crystallize in the monoclinic space groups *C*2/c and *P*2₁/n, respectively. Both consist of four Mn^{IV} and eight Mn^{III} ions held together by 10 μ₃O²⁻ ions, and either (i) one μ-OH⁻ and three μ-MeO⁻ groups for **1** or (ii) four μ-MeO⁻ groups for **2**. Complex **3** crystallizes in the orthorhombic space group *Aba*2 and possesses the normal Mn₁₂ structure but with terminal MeOH molecules. The cyclic voltammogram (CV) of **1** exhibits no reversible redox processes. Variable-temperature, solid-state dc and ac magnetic susceptibility measurements on **1** and **2** reveal that they possess *S* = 5 and 9 ground states, respectively. In addition, ac susceptibility measurements on complex **1** in a zero dc field in the temperature range 1.8–10 K and in a 3.5 G ac field oscillating at frequencies in the 5–1488 Hz range display a nonzero frequency-dependent out-of-phase (χ_M‘‘) signal at temperatures below 3 K, with the peak maxima lying at temperatures below 1.8 K. For complex **2**, two frequency dependent χ_M‘‘ signals are seen, one in the higher temperature range of 3–5 K and a second at lower temperatures with its peak maxima at temperatures below 1.8 K. Single-crystal magnetization vs dc field scans down to 0.04 K for **1**·8MeOH and **2** show hysteresis behavior at <1 K, confirming that both complexes are new examples of SMMs.

Introduction

The design of high-nuclearity manganese carboxylate clusters is still an important research area for scientists in various disciplines. This interest derives not only from the aesthetically pleasing nature of many of these species but also from the discovery that some of them function as nanoscale magnetic particles, or single-molecule magnets (SMMs).¹ Such molecules exhibit superparamagnet-like slow magnetization relaxation and thus behave as magnets below their blocking temperature (*T*_B), exhibiting hysteresis in magnetization versus dc field scans. This behavior results from the combination of a large ground spin state (*S*) with

a large and negative Ising (or easy-axis) type of magnetocranisotropy, as measured by the axial zero-field splitting parameter *D*. This leads to a significant barrier (*U*) to magnetization reversal, its maximum value given by *S*²|*D*| or (*S*² - 1/4)|*D*| for integer and half-integer spin, respectively.² However, in practice, quantum tunneling of the magnetization (QTM) through the barrier via higher lying *M*_S levels of the spin *S* manifold results in the actual or effective barrier (*U*_{eff}) being less than *U*. The first SMM discovered was [Mn₁₂O₁₂(O₂CMe)₁₆(H₂O)₄],^{2a} which possesses an *S* = 10 ground state; together with the continually growing family of [Mn₁₂O₁₂(O₂CR)₁₆(H₂O)₄] (*Mn*₁₂; R = various) molecules, these clusters (hereafter referred to as “normal Mn₁₂”) are still the best and most thoroughly studied SMMs to date.^{1–3} Examples of other manganese SMMs include Mn₂,⁴ Mn₄,⁵ Mn₆,⁶ Mn₉,⁷ Mn₁₆,⁸ Mn₁₈,⁹ Mn₂₁,¹⁰ Mn₂₂,¹¹ Mn₂₅,¹² Mn₃₀,¹³ and Mn₈₄.¹⁴

* To whom correspondence should be addressed. E-mail: christou@chem.ufl.edu. Tel.: +1-352-392-8314. Fax: +1-352-392-8757.

[†] University of Florida.

[‡] Laboratoire Louis Néel-CNRS.

(1) (a) Aromi, G.; Aubin, S. M. J.; Bolcar, M. A.; Christou, G.; Eppley, H. J.; Folting, K.; Hendrickson, D. N.; Huffman, J. C.; Squire, R. C.; Tsai, H.-L.; Wang, S.; Wemple, M. W. *Polyhedron* **1998**, *17*, 3005. (b) Christou, G.; Gatteschi, D.; Hendrickson, D. N.; Sessoli, R. *MRS Bull.* **2000**, *25*, 66. (c) Blundell, S. J.; Pratt, F. L. *J. Phys.: Condens. Matter* **2004**, *16*, R771.

(2) (a) Sessoli, R.; Gatteschi, D.; Caneschi, A.; Novak, M. A. *Nature* **1993**, *365*, 141. (b) Sessoli R.; Ysai, H. -L.; Schake, A. R.; Wang, S.; Vincent, J. B.; Folting, K.; Gatteschi, D.; Christou, G.; Hendrickson, D. N. *J. Am. Chem. Soc.* **1993**, *115*, 1804.

As part of our continuing search for new synthetic routes to such high-nuclearity manganese carboxylate clusters, we have recently developed a novel synthetic approach involving reductive aggregation of permanganate (MnO_4^-) ions in the presence of MeOH and excess carboxylic acid. In contrast to the usual comproportionation reaction between Mn^{II} and Mn^{VII} ions, as used in the synthesis of normal Mn_{12} molecules, this procedure represents a convenient, single-source route to high oxidation state Mn^{III} and/or Mn^{IV} polynuclear products. In this approach, a Mn^{II} source is

- (3) (a) Eppley, H. J.; Tsai, H.-L.; de Vries, N.; Folting, K.; Christou, G.; Hendrickson, D. N. *J. Am. Chem. Soc.* **1995**, *117*, 301. (b) Aubin, S. M. J.; Spagna, S.; Eppley, H. J.; Sager, R. E.; Christou, G.; Hendrickson, D. N. *Chem. Commun.* **1998**, 803. (c) Aubin, S. M. J.; Sun, Z.; Pardi, L.; Krzystek, J.; Folting, K.; Brunel, L.-C.; Rheingold, A. L.; Christou, G.; Hendrickson, D. N. *Inorg. Chem.* **1999**, *38*, 5329. (d) Soler, M.; Chandra, S. K.; Ruiz, D.; Davidson, E. R.; Hendrickson, D. N.; Christou, G. *Chem. Commun.* **2000**, 2417. (e) Boskovic, C.; Pink, M.; Huffman, J. C.; Hendrickson, D. N.; Christou, G. *J. Am. Chem. Soc.* **2001**, *123*, 9914. (f) Artus, P.; Boskovic, C.; Yoo, J.; Streib, W. E.; Brunel, L.-C.; Hendrickson, D. N.; Christou, G. *Inorg. Chem.* **2001**, *40*, 4199. (g) Soler, M.; Wernsdorfer, W.; Abboud, K. A.; Huffman, J. C.; Davidson, E. R.; Hendrickson, D. N.; Christou, G. *J. Am. Chem. Soc.* **2003**, *125*, 3576. (h) Chakov, N. E.; Abboud, K. A.; Zakharov, L. N.; Rheingold, A. L.; Hendrickson, D. N.; Christou, G. *Polyhedron* **2003**, *22*, 1759. (i) Brockman, J. T.; Abboud, K. A.; Hendrickson, D. N.; Christou, G. *Polyhedron* **2003**, *22*, 1765. (j) Soler, M.; Wernsdorfer, W.; Abboud, K. A.; Hendrickson, D. N.; Christou, G. *Polyhedron* **2003**, *22*, 1777. (k) Petukhov, K.; Hill, S.; Chakov, N. E.; Abboud, K. A.; Christou, G. *Phys. Rev. B: Condens. Matter. Mater. Phys.* **2004**, *70* (5), 054426. (l) Morello, A.; Bakharev, O. N.; Brom, H. B.; de Jongh, L. J. *Polyhedron* **2003**, *22*, 1745. (m) Mertes, K. M.; Suzuki, Y.; Sarachik, M. P.; Myasoedov, Y.; Shtrikman, H.; Zeldov, E.; Rumberger, E. M.; Hendrickson, D. N.; Christou, G. *J. Magn. Magn. Mater.* **2004**, 272. (n) Bian, G. -Q.; Kuroda-Sowa, T.; Konaka, H.; Hatano, M.; Maekawa, M.; Munakata, M.; Miyasaka, H.; Yamashita, M. *Inorg. Chem.* **2004**, *43*, 4790.
- (4) Miyasaka, H.; Clérac, R.; Wernsdorfer, W.; Leclerc, L.; Bonhomme, C.; Sugiura, K.; Yamashita, M. A. *Angew. Chem., Int. Ed.* **2004**, *43*, 2801.
- (5) (a) Aubin, S. M. J.; Wemple, M. W.; Adams, D. M.; Tsai, H. -L.; Christou, G.; Hendrickson, D. N. *J. Am. Chem. Soc.* **1996**, *118*, 7746. (b) Aubin, S. M.; Gilley, N. R.; Pardi, L.; Krzystek, J.; Wemple, M. W.; Brunel, L. C.; Marple, M. B.; Christou, G.; Hendrickson, D. N. *J. Am. Chem. Soc.* **1998**, *120*, 4991. (c) Brechin, E. K.; Yoo, J.; Huffman, J. C.; Hendrickson, D. N.; Christou, G. *Chem. Commun.* **1999**, 783. (d) Yoo, J.; Brechin, E. K.; Yamaguchi, A.; Nakano, M.; Huffman, J. C.; Maniero, A. L.; Brunel, L.-C.; Awaga, K.; Ishimoto, H.; Christou, G.; Hendrickson, D. N. *Inorg. Chem.* **2000**, *39*, 3615. (e) Yoo, J.; Yamaguchi, A.; Nakano, M.; Krzystek, J.; Streib, W. E.; Brunel, L.-C.; Ishimoto, H.; Christou, G.; Hendrickson, D. N. *Inorg. Chem.* **2001**, *40*, 4604. (f) Yang, E.; Harden, N.; Wernsdorfer, W.; Zakharov, L.; Brechin, E. K.; Rheingold, A. L.; Christou, G.; Hendrickson, D. N. *Polyhedron* **2003**, *22*, 1857. (g) Wittick, L. M.; Murray, K. S.; Moubaraki, B.; Batten, S. R.; Spiccia, L.; Berry, K. J. *J. Chem. Soc., Dalton Trans.* **2004**, *7*, 1003.
- (6) Milios, C. J.; Raptopoulou, C. P.; Terzis, A.; Lloret, F.; Vicente, R.; Perlepes, S. P.; Escuer, A. *Angew. Chem., Int. Ed.* **2003**, *43*, 210.
- (7) Brechin, E. K.; Soler, M.; Davidson, J.; Hendrickson, D. N.; Parsons, S.; Christou, G. *Chem. Commun.* **2002**, 2252.
- (8) Price, D. J.; Batten, S. R.; Moubaraki, B.; Murray, K. S. *Chem. Commun.* **2002**, 762.
- (9) Brechin, E. K.; Boskovic, C.; Wernsdorfer, W.; Yoo, J.; Yamaguchi, A.; Sanudo, E. C.; Concolino, T. R.; Rheingold, A. L.; Ishimoto, H.; Hendrickson, D. N.; Christou, G. C. *J. Am. Chem. Soc.* **2002**, *124*, 9710.
- (10) Sanudo, E. C.; Wernsdorfer, W.; Abboud, K. A.; Christou, G. *Inorg. Chem.* **2004**, *43*, 4137.
- (11) Murugesu, M.; Raftery, J.; Wernsdorfer, W.; Christou, G.; Brechin, E. K. *Inorg. Chem.* **2004**, *43*, 4203.
- (12) Murugesu, M.; Habrych, M.; Wernsdorfer, W.; Abboud, K. A.; Christou, G. *J. Am. Chem. Soc.* **2004**, *126*, 4766.
- (13) Soler, M.; Rumberger, E.; Folting, K.; Hendrickson, D. N.; Christou, G. *Polyhedron* **2001**, *20*, 1365.
- (14) Tasiopoulos, A. J.; Vinslave, A.; Wernsdorfer, W.; Abboud, K. A.; Christou, G. *Angew. Chem., Int. Ed.* **2004**, *43*, 2117.

omitted and MeOH is used as both the reducing agent for Mn^{VII} and as a potential source of MeO^- bridging ligands, in the presence also of excess carboxylic acid to prevent formation of manganese oxides and/or hydroxides. The first compound synthesized using this new method was $(\text{NBu}^n)_2[\text{Mn}_{12}\text{O}_{12}(\text{OMe})_2(\text{O}_2\text{CPh})_{16}(\text{H}_2\text{O})_2]$,¹⁵ which is a new type of Mn_{12} SMM with a flat central Mn_4 topology, hence the term “flat Mn_{12} ”. This is distinctly different from the central core of a “normal Mn_{12} ” complex, which has a tetrahedral Mn_4 topology within a cubic $[\text{Mn}_4\text{O}_4]$ unit. In addition, this procedure has also provided a series of $[\text{Mn}_{16}\text{O}_{16}(\text{OMe})_6(\text{O}_2\text{CR})_{16}(\text{MeOH})_6]$ ($\text{R} = \text{CH}_2\text{Ph}, \text{CH}_2\text{Cl}, \text{CH}_2\text{Br}$) complexes that we have published elsewhere.¹⁶

We herein describe the preparation, structure, and detailed magnetic properties of two new products from this approach that expand the family of “flat Mn_{12} ” complexes. As will be seen, these are both new SMMs. In addition, a new high-symmetry member of the normal Mn_{12} family is reported, which was also obtained from a reductive aggregation reaction of $\text{NBu}^n_4\text{MnO}_4$.

Experimental Section

Syntheses. All manipulations were performed under aerobic conditions using chemicals as received, unless otherwise stated. $\text{NBu}^n_4\text{MnO}_4$ was prepared as previously reported.¹⁷

$[\text{Mn}_{12}\text{O}_{10}(\text{OMe})_3(\text{OH})(\text{O}_2\text{CC}_6\text{H}_3\text{F}_2)_{16}(\text{MeOH})_2]$ (1·8MeOH). To a stirred solution of 3,5-difluorobenzoic acid (1.62 g, 20.5 mmol) in MeOH (5 mL) was added solid $\text{NBu}^n_4\text{MnO}_4$ (0.25 g, 0.7 mmol) in small portions, resulting in a dark purple solution which quickly turned dark brown. After being stirred for 5 min, the solution was left undisturbed at ambient temperature for 1 day, during which time grew large black crystals of $[\text{Mn}_{12}\text{O}_{10}(\text{OMe})_3(\text{OH})(\text{O}_2\text{CC}_6\text{H}_3\text{F}_2)_{16}(\text{MeOH})_2] \cdot 8\text{MeOH}$; the yield was 23 mg (11%). The crystals of **1·8MeOH** were maintained in the mother liquor for X-ray crystallography and other single-crystal studies or collected by filtration, washed with EtOH (MeOH causes precipitation), and dried in vacuo. The dried solid analyzed as fully desolvated. Anal. Calcd (found) for **1**: C, 40.07 (40.35); H, 1.90 (2.28). Selected IR data (KBr, cm^{-1}): 3430 (w), 3097 (m), 2968 (m), 1620 (s), 1583 (s), 1470 (s), 1441 (s), 1401 (m), 1307 (s), 1120 (s), 987 (s), 960 (s), 890 (s), 858 (s), 782 (s), 757 (s), 663 (s), 605 (m), 576 (s), 516 (m), 433 (m).

$[\text{Mn}_{12}\text{O}_{10}(\text{OMe})_4(\text{O}_2\text{CBu}^t)_{16}(\text{MeOH})_2]$ (2) and $[\text{Mn}_{12}(\text{O}_2\text{CBu}^t)_{16}(\text{MeOH})_4]$ (3). To a stirred solution of pivalic acid (2.09 g, 20.5 mmol) in MeOH (7.5 mL) was added solid $\text{NBu}^n_4\text{MnO}_4$ (0.50 g, 1.4 mmol) in small portions, resulting in a dark purple solution which quickly turned dark brown. After being stirred for 5 min, the solution was left undisturbed at ambient temperature for 2 days, during which time grew large black crystals of $[\text{Mn}_{12}\text{O}_{10}(\text{OMe})_4(\text{O}_2\text{CBu}^t)_{16}(\text{MeOH})_2]$ (**2**). The yield was 19 mg (6%). The crystals of **2** were maintained in the mother liquor for X-ray crystallography and other single-crystal studies or collected by filtration, washed with EtOH (MeOH causes precipitation), and dried in vacuo. Anal. Calcd (found) for dried **2**: C, 39.34 (39.59);

(15) (a) Tasiopoulos, A. J.; Wernsdorfer, W.; Abboud, K. A.; Christou, G. *Angew. Chem., Int. Ed.* **2004**, *43*, 6338. (b) Tasiopoulos, A. J.; Wernsdorfer, W.; Abboud, K. A.; Christou, G. *Inorg. Chem.*, in press.

(16) King, P.; Wernsdorfer, W.; Abboud, K. A.; Christou, G. *Inorg. Chem.* **2004**, *43*, 7315.

(17) (a) Sala, T.; Sargent, M. V. *Chem. Commun.* **1978**, 253. (b) Vincent, J. B.; Chang, H. R.; Folting, K.; Huffman, J. C.; Christou, G.; Hendrickson, D. N. *J. Am. Chem. Soc.* **1987**, *109*, 5703.

Table 1. Crystallographic Data for **1·8MeOH**, **2**, and **3**

param	1	2	3
formula ^a	$C_{124}H_{196}F_{32}Mn_{12}O_{56}$	$C_{86}H_{164}Mn_{12}O_{48}$	$C_{84}H_{124}Mn_{12}O_{48}$
fw ^a	3850.09	2625.45	2561.11
space group	$C2/c$	$P2_1/n$	$Aba2$
<i>a</i> , Å	30.222(2)	17.5287(9)	21.2382(13)
<i>b</i> , Å	21.10617(17)	19.1454(10)	29.4770(19)
<i>c</i> , Å	27.151(2)	20.4668(11)	19.4191(13)
α , deg	90	90	90
β , deg	116.817(2)	112.709(2)	90
γ , deg	90	90	90
<i>V</i> , Å ³	15 424(2)	6336.1(6)	12 157.1(14)
<i>Z</i>	4	2	4
<i>T</i> , K	173(2)	173(2)	173(2)
radiatn, ^b Å	0.710 73	0.710 73	0.710 73
ρ_{calc} , g/cm ³	1.658	1.376	1.399
μ , mm ⁻¹	1.070	1.228	1.278
R1 ^{c,d}	0.0752	0.0625	0.0556
wR2 ^e	0.1820	0.1553	0.0969

^a Not including solvate molecules. ^b Graphite monochromator. ^c $I > 2\sigma(I)$. ^d $R1 = 100\sum(|F_o| - |F_c|)/\sum|F_o|$. ^e $wR2 = 100[\sum(w(F_o^2 - F_c^2)^2)/\sum(w(F_o^2))^2]]^{1/2}$, $w = 1/[\sigma^2(F_o^2) + (ap)^2 + bp]$, where $p = [\max(F_o^2, O) + 2F_c^2]/3$.

H, 6.30 (6.61). Selected IR data (KBr, cm⁻¹): 3431 (w), 2962 (m), 2928 (m), 2872 (m), 1705 (m), 1590 (m), 1559 (s), 1532 (s), 1483 (s), 1459 (s), 1424 (m), 1362 (m), 1334 (m), 1229 (s), 1030 (m), 893 (m), 783 (s), 662 (m), 622 (s), 559 (m), 459 (s). The filtrate was maintained for a further 2 days, and this gave a small quantity of small black crystals of $[Mn_{12}O_{12}(O_2CBu^t)_8(MeOH)_4]$ (**3**). The crystals were maintained in the mother liquor for X-ray crystallography. Further analysis was not possible due to the small yield.

X-ray Crystallography. Data were collected on a Siemens SMART PLATFORM equipped with a CCD area detector and a graphite monochromator utilizing Mo K α radiation ($\lambda = 0.710\text{ }73\text{ \AA}$). Suitable crystals of **1·8MeOH**, **2**, and **3** were attached to glass fibers using silicone grease and transferred to a goniostat where they were cooled to 173 K for data collection. An initial search of reciprocal space revealed a monoclinic cell for both **1·8MeOH** and **2** and an orthorhombic cell for **3**; the choice of space groups $C2/c$, $P2_1/n$, and $Aba2$, respectively, were confirmed by the subsequent solution and refinement of the structures. Cell parameters were refined using up to 8192 reflections. A full sphere of data (1850 frames) was collected using the ω -scan method (0.3° frame width). The first 50 frames were remeasured at the end of data collection to monitor instrument and crystal stability (maximum correction on I was < 1%). Absorption corrections by integration were applied on the basis of measured indexed crystal faces. The structures were solved by direct methods in SHELXTL¹⁸ and refined on F^2 using full-matrix least squares. The non-H atoms were treated anisotropically, whereas the hydrogen atoms were placed in calculated, ideal positions and refined as riding on their respective carbon atoms.

The asymmetric unit of **1·8MeOH** consists of half the Mn_{12} cluster lying on an inversion center and four MeOH molecules of crystallization. The latter molecules were disordered and could not be modeled properly; thus, the SQUEEZE program, a part of the PLATON package of crystallographic software, was used to calculate the solvent disorder area and remove its contribution to the overall intensity data. A total of 843 parameters were included in the structure refinement using 6155 reflections with $I > 2\sigma(I)$ to yield R1 and wR2 of 7.52% and 18.20%, respectively.

For **2**, the asymmetric unit consists of half the Mn_{12} cluster located on an inversion center. All Bu^t groups, except the one on C25, are disordered and were refined in two sites each with their

occupancy factors dependently refined. The MeOH ligand in the asymmetric unit is also similarly disordered and refined. A total of 643 parameters were included in the structure refinement on F^2 using 41 593 reflections with $I > 2\sigma(I)$ to yield R1 and wR2 of 6.25% and 15.53%, respectively.

The asymmetric unit of **3** consists of half the Mn_{12} cluster lying on a 2-fold rotation axis. Five of the Bu^t groups were disordered, and each was refined in two sites with their occupancy factors dependently refined. A total of 639 parameters were included in the structure refinement on F^2 using 3879 reflections with $I > 2\sigma(I)$ to yield R1 and wR2 of 5.56% and 9.69%, respectively. Unit cell data and details of the structure refinements for **1·8MeOH**, **2**, and **3** are listed in Table 1.

Other Studies. Infrared spectra were recorded in the solid state (KBr pellets) on a Nicolet Nexus 670 FTIR spectrometer in the 400–4000 cm⁻¹ range. Elemental analyses (C, H, and N) were performed by the in-house facilities of the University of Florida Chemistry Department. Cyclic voltammetry was performed on 1 mmol solutions at a 100 mV/s scan rate with a BAS CV-50W voltammetric analyzer and a standard three-electrode assembly (glassy-carbon working electrode, Pt wire auxiliary electrode, Ag/AgNO₃ reference electrode), with 0.1 M NBuⁿ₄PF₆ as supporting electrolyte. Potentials are quoted versus the ferrocene/ferrocenium couple under the same conditions. Variable-temperature dc and ac magnetic susceptibility data were collected at the University of Florida using a Quantum Design MPMS-XL SQUID susceptometer equipped with a 7 T magnet and operating in the 1.8–300 K range. Samples were embedded in solid eicosane to prevent torquing. Magnetization vs field and temperature data were fit using the program MAGNET.¹⁹ Pascal's constants were used to estimate the diamagnetic correction, which was subtracted from the experimental susceptibility to give the molar paramagnetic susceptibility (χ_M). Studies at ultralow temperatures (< 1.8 K) were performed on single crystals at Grenoble, France, using an array of micro-SQUIDS.²⁰ The high sensitivity of this magnetometer allows the study of single crystals of the order of 10–500 μm ; the field can be applied in any direction by separately driving three orthogonal coils.

Results and Discussion

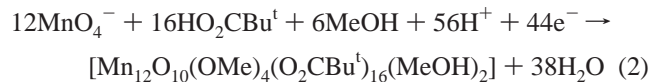
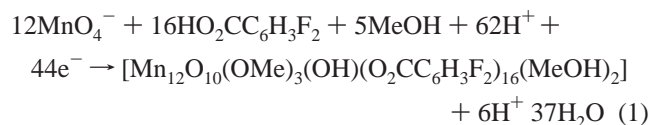
Syntheses. The reductive aggregation approach has so far proven to be a productive synthetic technique yielding several

(18) (a) Sheldrick, G. M. *SHELXL-97*; University of Göttingen: Göttingen, Germany, 1997. (b) Spek, A. L. *Acta Crystallogr., Sect. A* **1990**, *46*, C34.

(19) Davidson, E. R. *MAGNET*; Indiana University: Bloomington, IN, 1999.

(20) Wernsdorfer, W. *Adv. Chem. Phys.* **2001**, *118*, 99.

different types of Mn clusters. Variation of the carboxylic acid employed in the reaction has led to a “flat Mn_{12} ” complex $(NBu^n)_2[Mn_{12}O_{12}(OMe)_2(O_2CPh)_{16}(H_2O)_2]$ (**4**) with benzoic acid¹⁵ and Mn_{16} clusters with phenylacetic acid, chloroacetic acid, and bromoacetic acid.¹⁶ Subsequently a wide range of carboxylic acids has been explored and a variety of products have been obtained. For example, acetic acid yields the previously reported cluster $[Mn_{84}O_{72}(O_2CMe)_{78}(OMe)_{24}(MeOH)_{12}(H_2O)_{42}(OH)_6]$,¹⁴ *o*-toluic acid and 2-fluorobenzoic acid give normal Mn_{12} products, and 3,5-difluorobenzoic acid (**1·8MeOH**) and pivalic acid (**2**) give the two new flat Mn_{12} complexes reported here. However, for many of the other reactions investigated either (i) brown precipitates of manganese oxides/hydroxides were obtained or (ii) it did not prove possible to isolate clean products from the reaction solutions. These observations, together with the low yields of products such as **1** and **2**, make it clear that the reductive aggregation reactions are very complicated with an intricate mix of several species likely to be in equilibrium in the reaction solutions; this is perhaps to be expected given the nature of the reaction. Thus, factors such as relative solubility, lattice energies, crystallization kinetics, and others undoubtedly determine the identity of the isolated product, rationalizing the often large differences in products when the carboxylic acid was changed. The overall formation of complexes **1·8MeOH** and **2** is summarized in eqs 1 and 2, assuming single products:



The reducing equivalents are from the MeOH solvent, although we have not sought the presence of formaldehyde or formic acid in the reaction filtrates.

As was mentioned in our previous report,^{15,16} the small volume of MeOH employed in these reductive aggregation reactions was crucial for the attainment of these clusters. Brown precipitates of manganese oxides/hydroxides were obtained when more dilute solutions were used or if the acid-to- MnO_4^- ratio was decreased. Conversely, when the latter ratio was increased, bleaching of the reaction solution occurred, suggesting the formation of Mn^{II} species; this was also the case when EtOH was employed. Further investigation of the effect of changing the solvent revealed that the addition of dichloromethane as reaction cosolvent favored the production of normal Mn_{12} clusters.

It was also essential in these reductive aggregation reactions to use freshly prepared $NBu^n_4MnO_4$; otherwise only brown precipitates of manganese oxides/hydroxides were obtained. However, complexes **1·8MeOH** and **2** were also obtained when the $NBu^n_4MnO_4$ was replaced by $KMnO_4$, but we could not obtain complex **3** with the latter reagent.

Description of the Structures of **1·8MeOH, **2**, and **3**.** An ORTEP representation of the complete Mn_{12} molecule

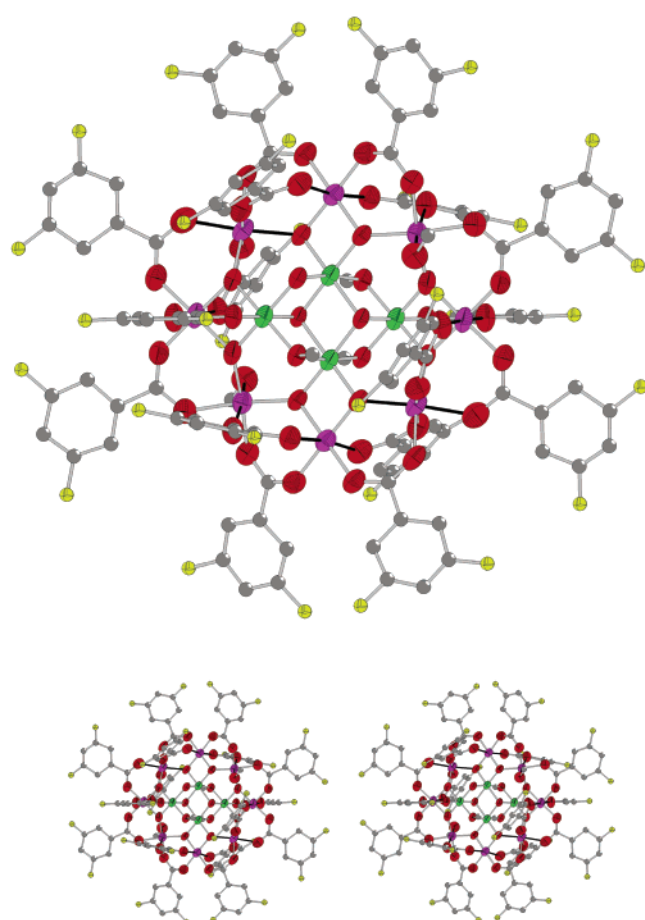


Figure 1. ORTEP representation and stereopair of **1·8MeOH** at the 50% probability level. Hydrogen atoms have been omitted for clarity. Solid black bonds denote Jahn–Teller elongation axes. Color code: Mn^{IV}, green; Mn^{III}, purple; O, red; Cl, yellow; C, gray.

of $[Mn_{12}O_{10}(OMe)_3(OH)(O_2CC_6H_3F_2)_{16}(MeOH)_2]·8MeOH$ (**1·8MeOH**) and a stereopair are provided in Figure 1. A labeled ORTEP representation of the core and a side view are provided for comparison with complexes **2** and **3** in Figure 2. Selected interatomic distances and angles are listed in Table 2.

Complex **1·8MeOH** crystallizes in the monoclinic space group *C*2/c with each Mn_{12} cluster on a *C*₂ rotation axis. The cluster contains four Mn^{IV} and eight Mn^{III} ions bridged by 10 μ_3 -O²⁻, 1 μ -OH⁻, 3 μ -MeO⁻, and 16 $C_6H_3F_2CO_2^-$ groups. The four Mn^{IV} ions, Mn3, Mn4, and their symmetry equivalents, are located within a central $[Mn^{IV}_4(\mu_3-O)_2(\mu-OH)(\mu-MeO)_3]^{4+}$ core, which can be described as a defect face-fused double-cubane with two missing metal vertexes, where the crystallographically related Mn3, Mn3', O3, and O3' occupy the four vertexes of the common face. The defect double-cubane core contains a planar flat Mn₄ rhombus. Although this dicubane-like core is relatively common for tetrานuclear species,^{5f–g,21} it is rarely seen in large manganese clusters. The few examples of the latter include Mn_{16} ,^{8,16} Mn_{21} ,^{10,22} Mn_{25} ,¹² and the related flat Mn_{12} complex **4**, the foundation of this work, which is described elsewhere.¹⁵

Encapsulating the defect double-cubane central core is a nonplanar ring of eight Mn^{III} atoms (Mn1, Mn2, Mn5, Mn6, and their symmetry equivalents) to which it is connected by

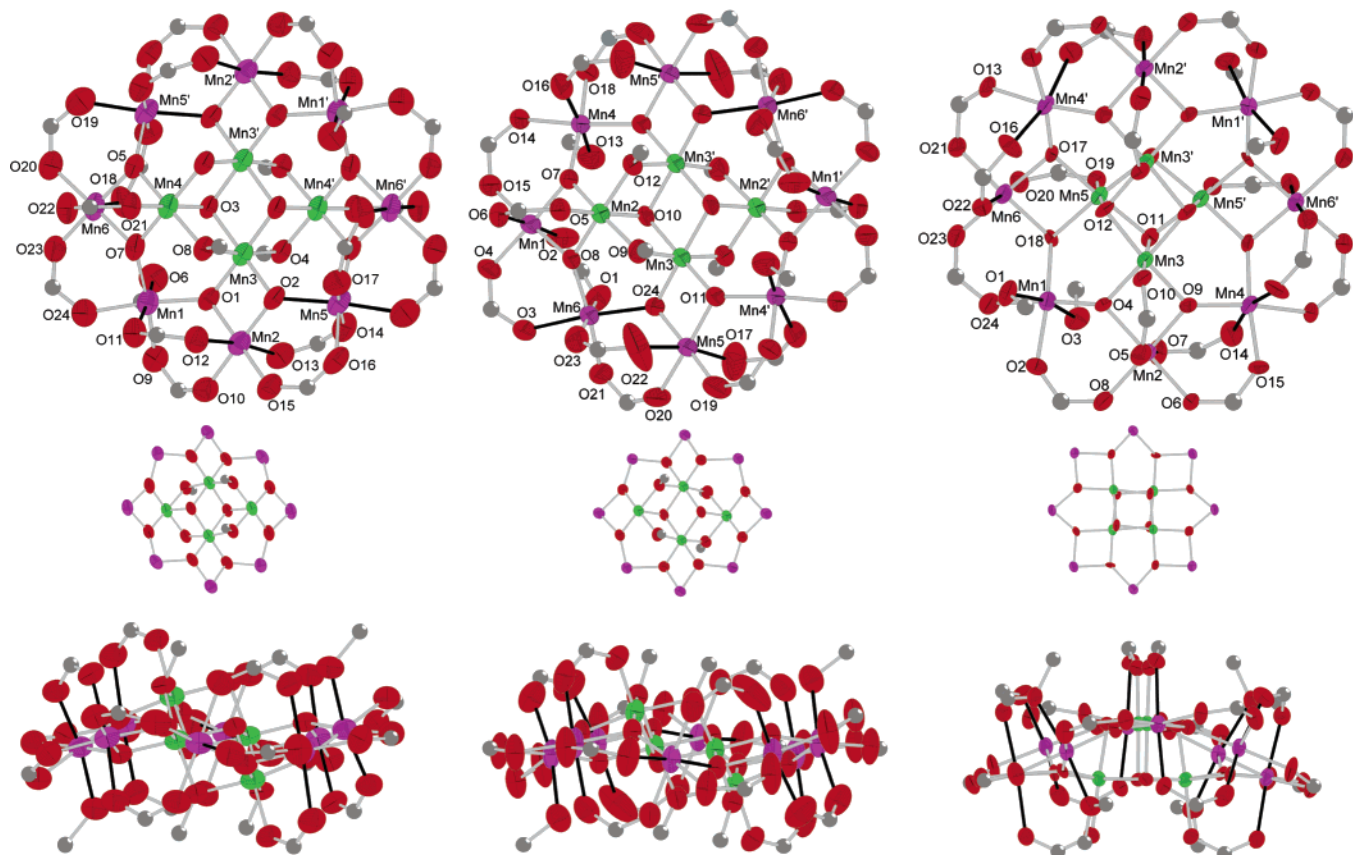


Figure 2. Comparison of the labeled ORTEP representations at the 50% probability level and front and side views of the cores for **1·8MeOH** (left), **2** (middle), and **3** (right). Solid black bonds denote Jahn–Teller elongation axes. Color code: Mn^{IV}, green; Mn^{III}, purple; O, red; C, gray.

eight $\mu_3\text{-O}^{2-}$ ions in the plane of the molecule. The 16 $\mu\text{-C}_6\text{H}_3\text{F}_2\text{CO}_2^-$ ligands and 2 terminal MeOH molecules provide the peripheral ligation of the complete complex, which has a chairlike conformation as can be seen from the side view in Figure 2.

The 12 Mn ions in **1·8MeOH** are all six-coordinate with near-octahedral geometry, and their assigned oxidation states were established by charge considerations, bond valence sum calculations (Table 3), and the clear Jahn–Teller (JT) distortions at the Mn^{III} ions. Mn1, Mn2, Mn6, and their symmetry equivalents have JT axial elongations with, as expected, the elongated Mn^{III}–O bonds being at least 0.1–0.2 Å longer than the other Mn^{III}–O bonds. In addition, these JT axes are in the “normal” orientation/position, pointing toward carboxylate O atoms and thus not along the core Mn–O²⁻ bonds, the shortest and strongest at the Mn^{III} ions. At

(21) (a) Li, H.; Zhong, Z. J.; Chen, W.; Tou, X. *J. Chem. Soc., Dalton Trans.* **1997**, 463. (b) Sunatsuki, Y.; Shimada, H.; Matsuo, T.; Nakamura, M.; Kai, F.; Matsumoto, N.; Re, N. *Inorg. Chem.* **1998**, 37, 5566. (c) Breeze, S. R.; Wang, S.; Creedan, J. E.; Raju, N. P. *J. Chem. Soc., Dalton Trans.* **1998**, 2327. (d) Clement-Juan, J. M.; Coronado, E.; Galan-Mascaros J. R.; Gomez-Garcia, C. J. *Inorg. Chem.* **1999**, 38, 55. (e) Benelli, C.; Murrie, M.; Parsons, S.; Winpenny, R. E. P. *J. Chem. Soc., Dalton Trans.* **1999**, 4125. (f) Serna, Z. E.; Urtiaga, M. K.; Barandika, M. G.; Cortes, R.; Martin, S.; Lezama, L.; Arriortua, M. I.; Rojo, T. *Inorg. Chem.* **2001**, 40, 4550. (g) Glaser, T.; Lugger, T. *Inorg. Chim. Acta* **2002**, 337, 103. (h) Karmakar, T. K.; Chandra, S. K.; Ribas, J.; Mostafa, G.; Lu, T. H.; Ghosh, B. K. *Chem. Commun.* **2002**, 2364. (i) King, P.; Clerac, R.; Wernsdorfer, W.; Anson, C. E.; Powell, A. K. *J. Chem. Soc., Dalton Trans.* **2004**, 17, 2670.

(22) Brockman, J. T.; Huffman, J. C.; Christou, G. *Angew. Chem., Int. Ed.* **2002**, 41, 2506.

Table 2. Selected Bond Distances (Å) and Angles (deg) for **1·8MeOH**

Mn1–O1	1.907(4)	Mn5–O14	2.001(5)
Mn1–O6	2.181(5)	Mn5–O16	1.971(5)
Mn1–O7	1.925(4)	Mn5–O17	2.037(5)
Mn1–O9	1.986(5)	Mn5–O19'	2.088(6)
Mn1–O11	2.086(4)	Mn6–O5	1.891(4)
Mn1–O24	2.013(5)	Mn6–O7	1.891(4)
Mn2–O1	1.917(3)	Mn6–O18	2.188(5)
Mn2–O2	1.872(4)	Mn6–O20	1.942(5)
Mn2–O10	1.958(5)	Mn6–O22	2.239(5)
Mn2–O12	2.193(4)	Mn6–O23	1.924(5)
Mn2–O13	2.191(5)	Mn1···Mn2	3.338(7)
Mn2–O15	1.989(4)	Mn1···Mn3	3.451(4)
Mn3–O1	1.899(4)	Mn1···Mn4	3.496(6)
Mn3–O2	1.873(4)	Mn1···Mn6	3.429(4)
Mn3–O3	1.910(4)	Mn2···Mn3	2.807(1)
Mn3–O4	1.885(3)	Mn2···Mn5	3.401(5)
Mn3–O8	1.913(3)	Mn3···Mn3'	2.944(4)
Mn3–O3'	1.943(3)	Mn3···Mn4	2.832(9)
Mn4–O3	1.877(3)	Mn3···Mn4'	2.856(4)
Mn4–O4'	1.890(4)	Mn3···Mn5	3.457(6)
Mn4–O5	1.862(4)	Mn4···Mn3'	2.835(5)
Mn4–O7	1.888(4)	Mn4···Mn6	2.769(8)
Mn4–O8	1.896(4)	Mn4···Mn5'	3.429(7)
Mn4–O21	1.936(4)	Mn5···Mn4'	5.453(5)
Mn5–O2	2.013(4)	Mn5···Mn6'	3.390(8)
Mn5–O5'	1.891(4)	Mn6···Mn5'	3.390(8)
Mn1–O1–Mn2	121.7(2)	Mn6–O7–Mn1	128.0(2)
Mn2–O2–Mn3	97.12(17)	Mn3–O2–Mn5	125.6(2)
Mn2–O2–Mn5	121.94(19)	Mn4–O7–Mn1	133.1(2)
Mn3–O1–Mn1	130.33(19)	Mn4–O3–Mn3	96.81(17)
Mn3–O1–Mn2	94.70(16)	Mn4–O3–Mn3'	96.78(16)
Mn3–O3–Mn3'	99.69(16)	Mn4–O8–Mn3	97.16(16)
Mn3–O4–Mn4	97.21(17)	Mn4–O5–Mn5'	132.1(2)
Mn4–O7–Mn6	94.25(19)	Mn4–O5–Mn6	95.12(18)
Mn6–O5–Mn5'	127.5(2)		

Table 3. Bond Valence Sums for the Mn Atoms in **1**·8MeOH, **2**, and **3^a**

atom	1			2			3		
	Mn ^{II}	Mn ^{III}	Mn ^{IV}	Mn ^{II}	Mn ^{III}	Mn ^{IV}	Mn ^{II}	Mn ^{III}	Mn ^{IV}
Mn(1)	3.14	2.87	3.01	3.33	3.04	3.20	3.10	2.83	2.97
Mn(2)	3.18	2.91	3.06	4.35	3.98	4.18	3.26	2.98	3.13
Mn(3)	4.07	3.73	3.91	4.29	3.92	4.12	4.15	3.79	3.98
Mn(4)	4.27	3.91	4.10	3.23	2.95	3.10	3.15	2.88	3.03
Mn(5)	3.22	2.95	3.09	3.32	3.04	3.19	4.27	3.91	4.10
Mn(6)	3.29	3.01	3.16	3.30	3.02	3.17	3.27	2.99	3.14

^a The bold value is the one closest to the charge for which it was calculated. The oxidation state of a particular atom can be taken as the whole number nearest to the bold value.

Table 4. Selected Bond Distances (Å) and Angles (deg) for **2**

Mn1–O2	2.191(5)	Mn5–O19	1.941(4)
Mn1–O4	1.920(4)	Mn5–O20	1.967(4)
Mn1–O6	2.202(5)	Mn5–O22	2.219(6)
Mn1–O7	1.901(3)	Mn5–O24	1.862(3)
Mn1–O8	1.892(3)	Mn6–O1	1.978(4)
Mn1–O15	1.927(4)	Mn6–O3	2.106(4)
Mn2–O5	1.909(4)	Mn6–O8	1.906(3)
Mn2–O7	1.851(3)	Mn6–O21	1.946(4)
Mn2–O8	1.844(3)	Mn6–O23	1.958(5)
Mn2–O9	1.907(4)	Mn6–O24	2.059(3)
Mn2–O10	1.887(3)	Mn1...Mn2	2.752(3)
Mn2–O12	1.912(3)	Mn1...Mn4	3.466(3)
Mn3–O9	1.875(4)	Mn1...Mn6	3.361(5)
Mn3–O10	1.905(3)	Mn2...Mn3	2.869(5)
Mn3–O10'	1.948(3)	Mn2...Mn3'	2.872(2)
Mn3–O11	1.870(3)	Mn2...Mn4	3.452(4)
Mn3–O12'	1.899(4)	Mn2...Mn6	3.439(5)
Mn3–O24	1.846(3)	Mn3...Mn2'	2.872(2)
Mn4–O7	1.918(3)	Mn3...Mn3'	2.934(4)
Mn4–O11'	1.902(3)	Mn3...Mn4'	3.415(6)
Mn4–O13	2.226(4)	Mn3...Mn5	2.795(3)
Mn4–O14	1.948(3)	Mn3...Mn6	3.491(4)
Mn4–O16	2.089(5)	Mn4...Mn3'	3.415(6)
Mn4–O18	1.977(4)	Mn4...Mn5'	3.311(3)
Mn5–O11	1.911(3)	Mn5...Mn4'	3.311(3)
Mn5–O17	2.119(5)	Mn5...Mn6	3.418(4)
Mn1–O7–Mn4	130.35(18)	Mn2–O10–Mn3	98.37(15)
Mn1–O8–Mn6	124.45(18)	Mn2–O10–Mn3'	97.01(15)
Mn2–O7–Mn1	94.36(14)	Mn3–O9–Mn2	98.68(18)
Mn2–O7–Mn4	132.62(16)	Mn3–O10–Mn3'	99.23(13)
Mn2–O8–Mn1	94.89(14)	Mn3–O11–Mn4	129.73(17)
Mn2–O8–Mn6	133.02(16)	Mn3–O11–Mn5	95.32(14)
Mn3–O12'–Mn2'	97.80(17)	Mn5–O11–Mn4'	120.54(16)
Mn3–O24–Mn5	97.83(14)	Mn5–O24–Mn6	121.20(15)
Mn3–O24–Mn6	126.67(16)		

the remaining Mn^{III} ions, Mn5 and its symmetry equivalent, there is again a JT elongation but with the elongation axis in an “abnormal” orientation, pointing toward O²⁻ ions O2. We reach this conclusion on the basis of the significant difference between the two Mn5–O²⁻ bonds, Mn5–O2 (2.013(4) Å), and Mn5–O5' (1.891(4) Å); the latter is typical of a Mn^{III}–O²⁻ bond, whereas the former is unusually long and indicative of a JT elongation. Such abnormally oriented JT elongation axes have been seen previously on several occasions for normal Mn₁₂ complexes, where they have been found to have a significant effect on the magnetic properties (vide infra).²³ Finally, as can be seen in Figure 2, the JT elongation axes at Mn1, Mn2, and Mn6 are aligned roughly parallel to each other and perpendicular to the abnormal JT axes.

(23) (a) Sun, Z.; Ruiz, D.; Dilley, N. R.; Soler, M.; Ribas, J.; Folting, K.; Maple, M. B.; Christou, G.; Hendrickson, D. N. *Chem. Commun.* **1993**, 1973. (b) Soler, M.; Wernsdorfer, W.; Sun, Z.; Huffman, J. C.; Hendrickson, D. N.; Christou, G. *Chem. Commun.* **2003**, 2672.

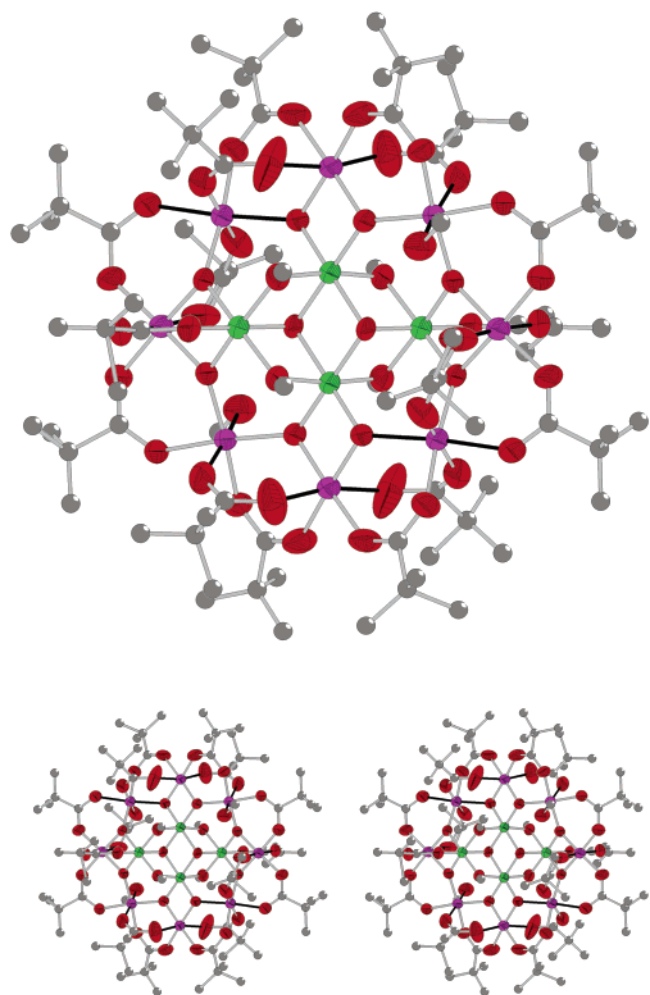


Figure 3. ORTEP representation and stereopair of **2** at the 50% probability level. Hydrogen atoms have been omitted for clarity. Solid black bonds denote Jahn–Teller elongation axes. Color code: Mn^{IV}, green; Mn^{III}, purple; O, red; C, gray.

An ORTEP representation of the complete Mn₁₂ molecule of **2** and a stereopair are provided in Figure 3. A labeled ORTEP of the core and a side view are provided for comparison with **1**·8MeOH and **3** in Figure 2. Selected interatomic distances and angles are listed in Table 4. Complex **2** crystallizes in the monoclinic space group *P2₁/n* with the Mn₁₂ cluster located on an inversion center. The cluster is analogous to **1** in that it has a central face-fused defect-dicubane core of four Mn^{IV} ions held within a nonplanar ring of eight Mn^{III} ions to give an overall chairlike conformation. However, a major difference between **2** and **1** is in the alkoxide-bridging of the central core; there are now four μ-MeO⁻ groups bridging the four Mn^{IV} ions to give a core of formula [Mn^{IV}₄(μ₃-O)₂(μ-OEt)₄]⁸⁺, in contrast to the [Mn^{IV}₄(μ₃-O)₂(μ-OEt)₃(μ-OH)]⁸⁺ core of **1**·8MeOH. Again, all eight Mn^{III} ions (Mn1, Mn4, Mn5, Mn6, and their symmetry equivalents) exhibit Jahn–Teller axial elongations with the JT elongated Mn^{III}–O bonds (2.059(3)–2.226(4) Å) being significantly longer than the other Mn^{III}–O bonds (1.862(3)–1.978(4) Å). For Mn1, Mn4, and Mn5 (and their symmetry equivalents), the JT elongation axes are aligned roughly parallel to each other and perpendicular to the plane of the cluster (Figure 2). In contrast, for Mn6 and its

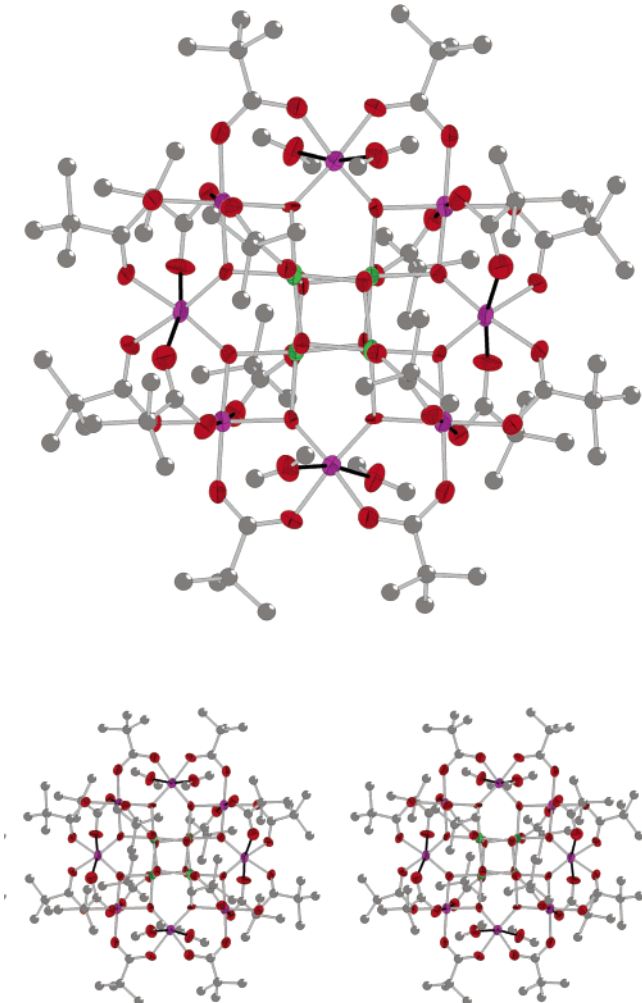


Figure 4. ORTEP representation and stereopair of **3** at the 50% probability level. Hydrogen atoms have been omitted for clarity. Solid black bonds denote Jahn–Teller elongation axes. Color code: Mn^{IV}, green; Mn^{III}, purple; O, red; C, gray.

symmetry equivalent, the JT elongation axes are aligned abnormally, being in the plane of the core i.e perpendicular to the six other JT elongation axes (Figure 2). This situation is thus similar to that in complex **1**·8MeOH.

An ORTEP representation of the complete Mn_{12} molecule of **3** and a stereopair are provided in Figure 4. A labeled ORTEP of the core and a side view are provided for comparison with **1**·8MeOH and **2** in Figure 2. Selected interatomic distances and angles are listed in Table 5. Complex **3** crystallizes in the orthorhombic space group *Aba*2 with each Mn_{12} cluster on a *C*₂ rotation axis. The cluster is of the well-known “normal Mn_{12} ” variety, with a central oxide-bridged $[Mn^{IV}_4(\mu_3\text{-O})_4]^{8+}$ cubane core held within a nonplanar ring of eight Mn^{III} ions by eight $\mu\text{-MeO}^-$ groups. The peripheral ligation is provided by 16 $\mu\text{-Bu}'\text{CO}_2^-$ ligands and 4 terminal MeOH molecules located on 2 Mn atoms. As can be seen from the side view in Figure 2, the complete complex has a slightly discus shape. All the Mn^{III} ions are six-coordinate with near-octahedral geometry, and their assigned oxidation states were established by charge considerations, bond valence sum calculations (Table 3), and the clear Jahn–Teller (JT) distortions of the Mn^{III} ions, which take the form of axial elongations. The JT elongated Mn^{III}–O

Table 5. Selected Bond Distances (Å) and Angles (deg) for **3**

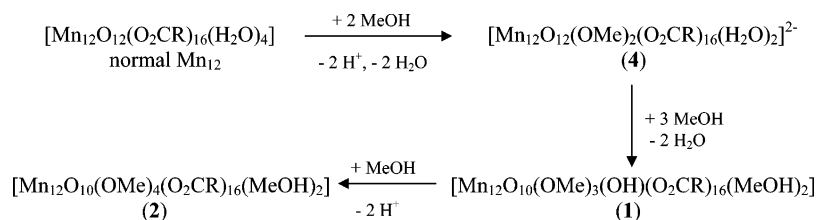
Mn1–O1	2.205(7)	Mn5–O17	1.891(5)
Mn1–O2	1.955(7)	Mn5–O18	1.886(6)
Mn1–O3	2.221(7)	Mn5–O19	1.951(7)
Mn1–O4	1.878(6)	Mn6–O17	1.881(6)
Mn1–O18	1.873(6)	Mn6–O18	1.908(6)
Mn1–O24	1.956(7)	Mn6–O20	2.153(8)
Mn2–O4	1.912(6)	Mn6–O21	1.947(7)
Mn2–O5	2.212(8)	Mn6–O22	2.173(8)
Mn2–O6	1.937(7)	Mn6–O23	1.934(8)
Mn2–O7	2.172(8)	Mn1···Mn2	3.403(2)
Mn2–O8	1.935(8)	Mn1···Mn3	3.446(2)
Mn2–O9	1.860(6)	Mn1···Mn5	3.457(3)
Mn3–O4	1.886(7)	Mn1···Mn6	3.406(2)
Mn3–O9	1.864(6)	Mn2···Mn3	2.795(2)
Mn3–O10	1.924(7)	Mn2···Mn4	3.316(3)
Mn3–O11	1.930(7)	Mn3···Mn4	3.448(2)
Mn3–O12	1.896(7)	Mn3···Mn5	2.825(2)
Mn3–O12'	1.918(6)	Mn3···Mn3'	2.947(3)
Mn4–O9	1.884(6)	Mn3···Mn5'	2.835(2)
Mn4–O13'	1.937(7)	Mn4···Mn3'	3.472(2)
Mn4–O14	2.155(9)	Mn4···Mn6'	3.320(3)
Mn4–O15	1.962(7)	Mn5···Mn6	2.802(2)
Mn4–O16'	2.152(9)	Mn5···Mn3'	2.835(2)
Mn4–O17'	1.896(6)	Mn5···Mn4'	3.472(2)
Mn5–O11	1.908(7)	Mn5···Mn5'	2.980(3)
Mn5–O11'	1.934(5)	Mn6···Mn4'	3.320(3)
Mn5–O12	1.893(7)		
Mn1–O4–Mn2	127.8(3)	Mn2–O9–Mn4	124.7(3)
Mn1–O4–Mn3	132.5(3)	Mn3–O4–Mn2	94.7(3)
Mn1–O18–Mn5	133.7(3)	Mn3–O12–Mn3'	101.2(3)
Mn1–O18–Mn6	128.5(3)	Mn3–O9–Mn4	133.9(3)
Mn2–O9–Mn3	97.3(3)	Mn3–O12–Mn5	96.4(3)
Mn3–O11–Mn5'	94.4(3)	Mn5–O11–Mn5'	101.7(3)
Mn5–O11–Mn3	94.8(3)	Mn5–O18–Mn6	95.2(3)
Mn5–O12–Mn3'	96.1(3)	Mn6–O17–Mn4'	123.1(3)
Mn5–O17–Mn4'	132.9(3)	Mn6–O17–Mn5	96.0(3)

bonds (2.152(9)–2.221(7) Å) are significantly longer than the other Mn^{III}–O bonds (1.860(6)–1.962(7) Å) and are aligned roughly parallel to one another, perpendicular to the plane of the cluster. Although some physical properties of this Mn_{12} analogue have previously been reported,²⁴ this is the first report to our knowledge of its crystal structure. In addition, we have recently discovered and communicated that high-symmetry Mn_{12} clusters can give extremely detailed magnetic information,²⁵ hence meriting further investigation of **3**.

Structural Comparison of Complexes 1–4. The structures of **1** and **2** are overall very similar to each other, differing only in the nature of one bridging ligand in the core, and also very similar to that of previously reported complex **4**, which has more oxides in the core (vide infra). The latter has the same flat Mn_{12} core comprising a defect-dicubane as **1** and **2** but retains a total of four core O²⁻ ions and thus has only two $\mu\text{-MeO}^-$ groups; i.e., it has a $[\text{Mn}_4\text{-}(\mu_3\text{-O})_2\text{-}(\mu\text{-O}_2)\text{-}(\mu\text{-OMe})_2]$ core. The structure of **1** and **2** is also somewhat similar to that of normal $[\text{Mn}_{12}\text{O}_{12}(\text{O}_2\text{CR})_{16}\text{-}(\text{H}_2\text{O})_4]$ complexes, as emphasized in Figure 2. All three clusters in Figure 2 comprise a nonplanar Mn^{III}₈ ring around a central Mn^{IV}₄ unit, but it is within this central core that the structural differences between the complexes lie. For

(24) Gerbier, P.; Ruiz-Molina, D.; Domingo, N.; Amabilino, D. B.; Vidal-Gancedo, J.; Tejada, J.; Hendrickson, D. N.; Veciana, J. *Monatsh. Chem.* **2003**, 134, 265.

(25) Harter, A. G.; Chakov, N. E.; Roberts, B.; Achey, R.; Reyes, A.; Kuhns, P.; Christou, G.; Dalal, N. S. *Inorg. Chem.* **2005**, 44, 2122.

Scheme 1

normal $[\text{Mn}_{12}\text{O}_{12}(\text{O}_2\text{CR})_{16}(\text{H}_2\text{O})_4]$ complexes such as **3**, the central Mn^{IV}_4 unit takes the form of an $[\text{Mn}_4\text{O}_4]$ cubane (and thus a tetrahedral Mn_4 topology), whereas in **1**, **2**, and **4**, alkoxide bridges have been introduced, the core has in effect been flattened to a defect-dicubane, and the Mn_4 unit is thus a rhombus.

Further consideration of the structural difference within the cores of **1–4** suggests that **1**, **2**, and **4** can be considered the result of progressive methanolysis of the central $[\text{Mn}_4\text{O}_4]^{8+}$ cubane of a normal $[\text{Mn}_{12}\text{O}_{12}(\text{O}_2\text{CR})_{16}(\text{H}_2\text{O})_4]$, leading to progressive incorporation of alkoxide bridges and a change in the core structure. We wish to emphasize that this is merely a structural comparison, and we are not claiming that the flat Mn_{12} complexes are forming in the reaction solutions from a methanolysis of normal Mn_{12} species; we have been unable to convert normal Mn_{12} species into flat Mn_{12} ones by dissolution in MeOH and have in fact found the reverse conversion to be favored. Nevertheless, progressive methanolysis does provide a useful way of relating the structures of **1–4**. This is summarized in Scheme 1.

Conversion of a normal Mn_{12} species to **4** involves opening up the $[\text{Mn}_4(\mu_3\text{-O})_4]$ cubane core by adding two MeO^- bridges to give a $[\text{Mn}_4(\mu_3\text{-O})_2(\mu\text{-O})_2(\mu\text{-OMe})_2]$ defect-dicubane. Replacement of one of the two $\mu\text{-O}^{2-}$ bridges of **4** with a $\mu\text{-MeO}^-$ and protonation of the remaining one then gives **1**, and then replacement of the $\mu\text{-OH}^-$ with a fourth $\mu\text{-MeO}^-$ gives **2**.

Electrochemical Studies on Complex 1. The redox properties of complex **1**·8MeOH were investigated by cyclic voltammetry in CH_2Cl_2 . The resulting cyclic voltammogram displays no reversible features and only one broad irreversible reduction at roughly -1.0 V , signifying the instability of **1**. This type of behavior is typical for high-nucularity Mn carboxylate aggregates; reversible redox processes are rarely seen. The normal Mn_{12} family represents one of the few examples of a higher nucularity species that does exhibit reversible redox processes.^{2b,3a,g,26}

Dc Magnetic Susceptibility Studies for Complexes 1 and 2. Solid-state variable-temperature magnetic susceptibility measurements were performed on vacuum-dried microcrystalline samples of complexes **1** and **2**, both suspended in eicosane to prevent torquing. The dc magnetic susceptibility (χ_M) data were collected in the $5.0\text{--}300 \text{ K}$ range in a 0.1 T magnetic field and are plotted as $\chi_M T$ vs T in Figure 5. For **1**, $\chi_M T$ steadily decreases with decreasing temperature

from $19.36 \text{ cm}^3 \text{ mol}^{-1} \text{ K}$ at 300 K to a minimum of $15.15 \text{ cm}^3 \text{ mol}^{-1} \text{ K}$ at 90 K and then increases to reach a maximum of $16.97 \text{ cm}^3 \text{ mol}^{-1} \text{ K}$ at 15 K , before dropping to $15.70 \text{ cm}^3 \text{ mol}^{-1} \text{ K}$ at 5.0 K . For **2**, $\chi_M T$ gradually decreases from $20.66 \text{ cm}^3 \text{ mol}^{-1} \text{ K}$ at 300 K to $17.42 \text{ cm}^3 \text{ mol}^{-1} \text{ K}$ at 150 K and then increases to a maximum of $38.09 \text{ cm}^3 \text{ mol}^{-1} \text{ K}$ at 6.5 K before decreasing again to $37.94 \text{ cm}^3 \text{ mol}^{-1} \text{ K}$ at 5.0 K . For both complexes, the value of $\chi_M T$ at 300 K is much lower than that expected for a cluster of 12 noninteracting Mn^{III} and Mn^{IV} ions ($31.5 \text{ cm}^3 \text{ mol}^{-1} \text{ K}$ for $g = 2$), suggesting the presence of overall strong, predominantly antiferromagnetic exchange interactions within the molecules. $\chi_M T$ vs T values for the two complexes are clearly very different, and the values at 5.0 K (assuming they are not unduly affected by Zeeman effects from the dc field and/or extensive population of excited states) are in the regions expected for $S = 5$ or 6 for **1**, and $S = 8$ or 9 for **2**.

With eight Mn^{III} and four Mn^{IV} centers in **1** and **2**, total spin values range from 0 to 22. However, due to the size and low symmetry of the molecules, a matrix diagonalization method to evaluate the various Mn pairwise exchange parameters (J_{ij}) within the Mn_{12} molecules is not easy. Similarly, application of the equivalent operator approach on the basis of the Kambe vector coupling method²⁷ is not possible. Therefore, we focused only on identifying the ground-state S value, as in any case this would dominate the ultralow-temperature studies we performed (vide infra). Hence, magnetization (M) data were collected in the magnetic field and temperature ranges $0.1\text{--}7 \text{ T}$ and $1.8\text{--}10 \text{ K}$ to

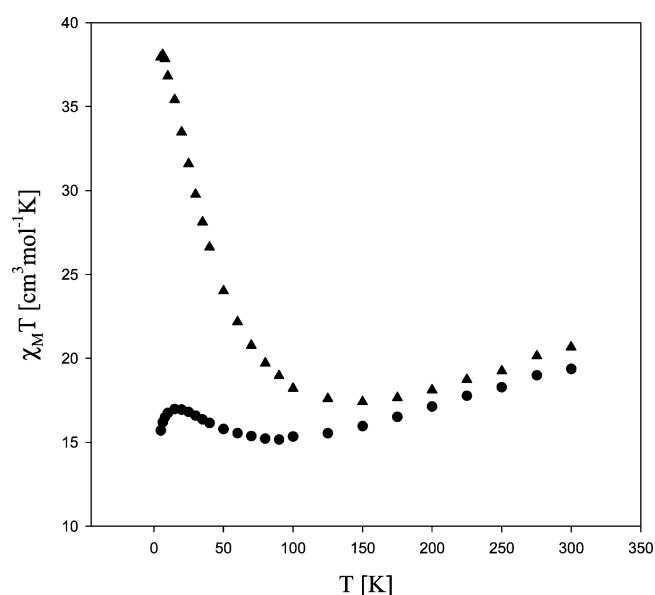


Figure 5. Plots of $\chi_M T$ vs T for complexes **1** (●) and **2** (▲).

(26) (a) Schake, A. R.; Tsai, H.-L.; Vries, N.; Webb, R. J.; Folting, K.; Hendrickson, D. N.; Christou, G. *Chem. Commun.* **1992**, 181. (b) Park, C.-D.; Jung, D.-Y. *Bull. Korean Chem. Soc.* **2001**, 22, 611. (c) Soler, M.; Chandra, S. K.; Ruiz, D.; Huffman, J. C.; Hendrickson, D. N.; Christou, G. *Polyhedron* **2001**, 1279.

determine the spin ground states of complexes **1** and **2**. Attempts to fit the resulting data using the program MAGNET,¹⁹ which assumes that only the ground state is populated at these temperatures, includes axial zero-field splitting (ZFS) and the Zeeman interaction with the applied field, and carries out a full powder average, did not lead to a good fit of the data for either of the complexes. This suggests that low-lying excited states are populated, even at these relatively low temperatures, and/or the M_S levels from nearby excited states with S greater than that of the ground state are being sufficiently stabilized by the applied dc field that they thus approach or even cross the ground state levels; note that the fitting model assumes population of only ground-state levels. Therefore, we turned to the use of more reliable methods based on ac magnetic susceptibility measurements,^{9,10,13} which do not employ a dc field, to identify the ground-state spins of **1** and **2**.

Ac Magnetic Susceptibility Studies on Complexes **1 and **2**.** Alternating current magnetic susceptibility studies were performed on vacuum-dried microcrystalline samples of **1** and **2** in the temperature range 1.8–10 K with a zero dc field and a 3.5 G ac field oscillating at frequencies between 5 and 1488 Hz. As seen in Figure 6 (top), the in-phase (χ_M') component of the ac susceptibility (plotted as $\chi_M'T$ vs T) for **1** at four frequencies (250, 498, 997, and 1488 Hz) decreases with temperature down to 3.5 K and then decreases more rapidly due to the onset of slow magnetization relaxation (vide infra). The decrease at temperatures above 3.5 K is suggestive of the population of low-lying excited states with S values greater than the ground-state S . Thus, as the temperature is lowered and excited states become depopulated, $\chi_M'T$ decreases. Extrapolation of the data from above 3.5 K to 0 K, where only the ground state will be populated, gives a $\chi_M'T$ of $\sim 14.5\text{ cm}^3\text{ mol}^{-1}\text{ K}$. This indicates an $S = 5$ ground state, since the spin-only ($g = 2.0$) value for $S = 5$ is $15\text{ cm}^3\text{ mol}^{-1}\text{ K}$ and $g < 2$ slightly is expected for Mn. Note that significant intermolecular interactions would make this extrapolation unreliable, but we see no significant intermolecular exchange pathways in **1**, only some weak F \cdots H–C contacts at the periphery of the molecules. In addition, the ground-state value obtained here is satisfactorily consistent with the estimate from the dc data in Figure 5. Note also that the use of wet (with mother liquor) crystals of **1**·8MeOH instead of vacuum-dried (desolvated) samples gave essentially the same ac data, so in this case the loss of solvent of crystallization does not significantly affect the magnetic properties.

At temperatures < 3.5 K, the $\chi_M'T$ value shows a frequency-dependent drop, concomitant with appearance of frequency-dependent χ_M'' signals (Figure 6, bottom). The latter show frequency-dependent tails of signals whose peaks lie at temperatures below the operating limit of our SQUID (1.8 K). Such frequency dependent ac signals are an indication of the superparamagnet-like slow relaxation of a SMM, although they do not prove an SMM because

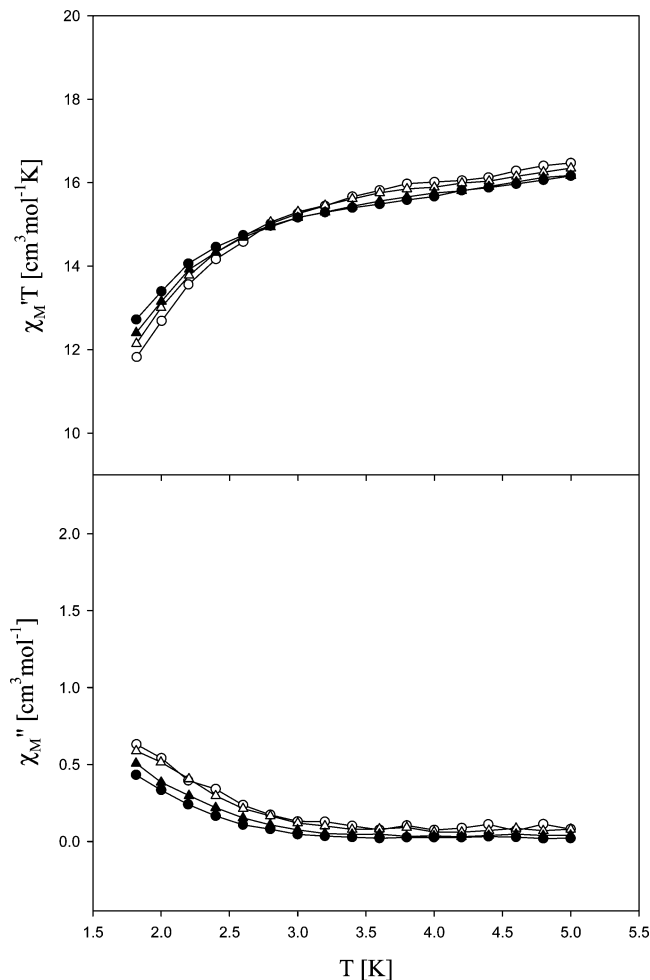


Figure 6. In-phase ac susceptibility signals (χ_M'), plotted as $\chi_M'T$, vs T (top) and out-of-phase ac susceptibility signals (χ_M'') vs T (bottom) for dried complex **1** at 250 (●), 498 (▲), 997 (△), and 1488 (○) Hz.

intermolecular interactions and phonon bottlenecks can also lead to such signals.²⁸

The ac susceptibility at four frequencies (250, 498, 997, and 1488 Hz) for complex **2** is shown in Figure 7, and it is clearly different from that seen for **1**. Two species are apparent in both the in-phase $\chi_M'T$ (plotted as $\chi_M'T$ vs T) (Figure 7, top) and out-of-phase χ_M'' (Figure 7, bottom) components of the ac susceptibility. This can most clearly be seen in the χ_M'' versus T plot where two frequency-dependent signals, a minority one in the higher temperature (HT) range of 3–5 K and a second, majority signal at lower temperatures (LT) whose peaks occur at temperatures below the operating limit of our SQUID instrument. This again indicates that **2**, like **1**, might be a SMM. As for **1**, note that use of wet crystals instead of vacuum-dried ones gave the same two peaks in comparable ratios—of course, crystals of **2** contain no solvent of crystallization, so it is not surprising that drying does not have a significant effect on the magnetic properties. Note that there is even a very small third signal in Figure 7 at ~ 6 K from a third species. The different χ_M'' signals are most probably due to different molecular environments within the crystal leading to varying relaxation rates.

(27) Kambe, K. *J. Phys. Soc. Jpn.* **1950**, *48*, 15.

(28) Chakov, N. E.; Wernsdorfer, W.; Abboud, K. A.; Christou, G. *Inorg. Chem.* **2004**, *43*, 5919.

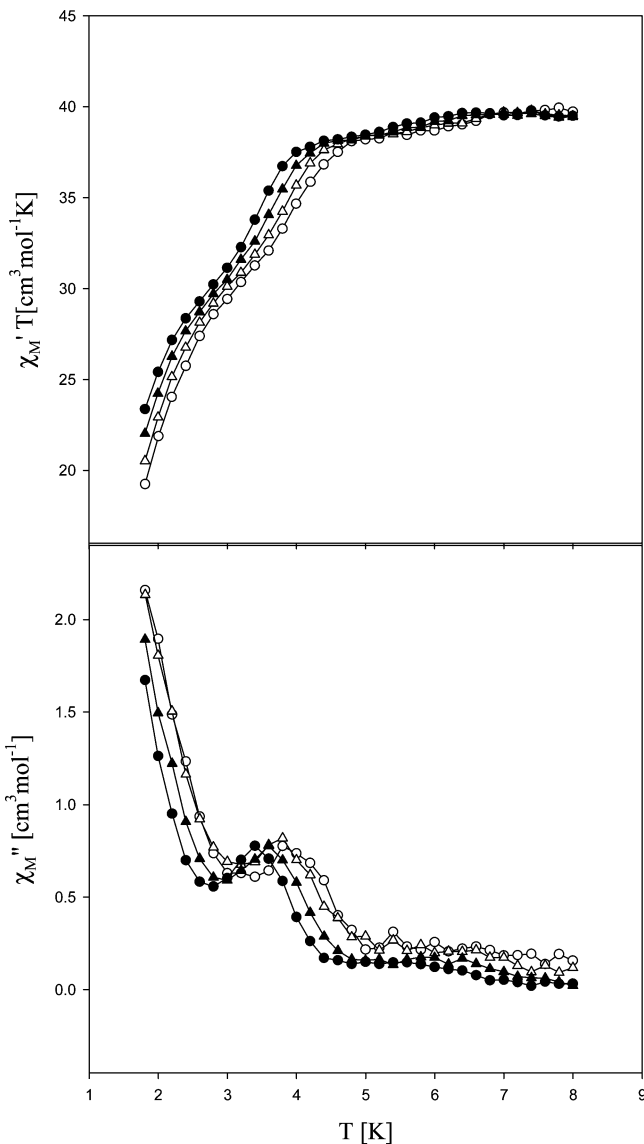


Figure 7. In-phase ac susceptibility signals (χ_M'), plotted as $\chi_M' T$, vs T (top) and out-of-phase ac susceptibility signals (χ_M'') vs T (bottom) for dried complex **2** at 250 (●), 498 (▲), 997 (△), and 1488 (○) Hz.

This behavior is analogous to that seen for the previously reported flat Mn_{12} complex **4** where it was found that faster- and slower-relaxing forms of the complex cocrystallize in the same crystal.¹⁵ The LT majority signal is assigned as due to the form detected crystallographically as possessing a JT elongation axis at Mn6 and its symmetry partner that is abnormally oriented in the plane of the molecule i.e., pointing toward oxide ion O24. It is known from previous work with so-called “JT isomers” among the normal Mn_{12} family (i.e. molecules differing in the relative orientation of one or more JT distortion axes)²³ that an abnormally oriented JT elongation axis pointing toward a core oxide ion leads to a faster relaxing (LT) form of the molecule. This would thus be consistent with the conclusion that the strong LT signal at <1.8 K is due to the crystallographic form in which Mn6 and its symmetry partner have abnormally oriented JT axes. The signal in the 3–4 K range would then perhaps be due to a small fraction of molecules in which only one of the JT axes is abnormally oriented and, thus, is a slower-relaxing

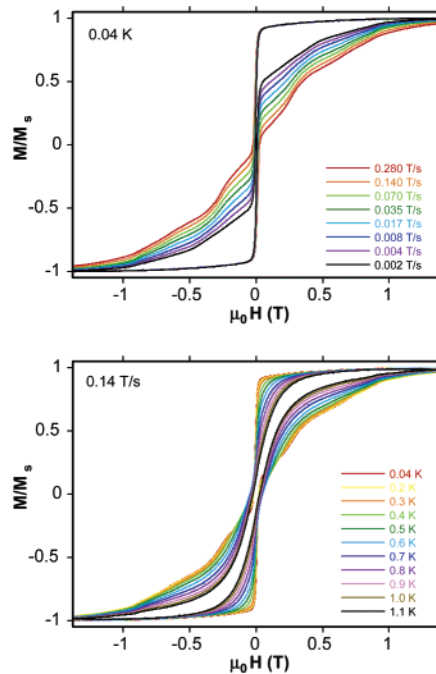


Figure 8. Magnetization (M) vs applied magnetic field hysteresis loops for **1**: (top) in the 0.002–0.280 T/s sweep rate range at 0.04 K; (bottom) in the temperature range 0.04–1.1 K at a 0.14 T/s sweep rate. M is normalized to its saturation value, M_s , for both plots.

(HT) form. Upon extension of this idea further, the very weak signal at ~ 6 K might then be molecules in which all JT elongation axes are oriented in the normal way, avoiding the core oxide ions. This is merely speculation at the present and will require further study and the crystallization of various forms of **2** to allow a correlation of JT axis orientation with magnetic properties before the situation can be sorted out as clearly as has been done for the normal Mn_{12} family. Note, however, that with the latter it is a common observation to see more than one JT isomeric form in the ac susceptibility plots, so the occurrence of more than one signal in Figure 7 is not surprising and may well also be due to different isomeric forms of **2**.

If we assume the smaller signals in Figure 7 are minor contributors to the total in-phase $\chi_M' T$, then extrapolating this to zero from temperatures above where the decreases due to slow relaxation occur gives a $\chi_M' T$ of ~ 40 cm³ mol⁻¹ K, indicating a $S = 9$ ground state and $g < 2$ slightly. Again, this is satisfactorily consistent with the estimate from Figure 5.

Since both **1** and **2** exhibit χ_M'' signals suggesting that they might be SMMs, lower temperature studies were carried out to explore this possibility further.

Hysteresis Studies. Magnetization vs applied dc field data down to 0.04 K were collected on single crystals of **1**·8MeOH and **2** using a micro-SQUID apparatus.²⁰ The observation of hysteresis loops in such studies represents the diagnostic property of a magnet, including SMMs and superparamagnets below their blocking temperature (T_B). The observed magnetization responses for complexes **1**·8MeOH and **2** at different field sweep rates and a constant temperature are shown in Figures 8 (top) and 9 (top). The corresponding magnetization responses for **1**·8MeOH and **2** at different

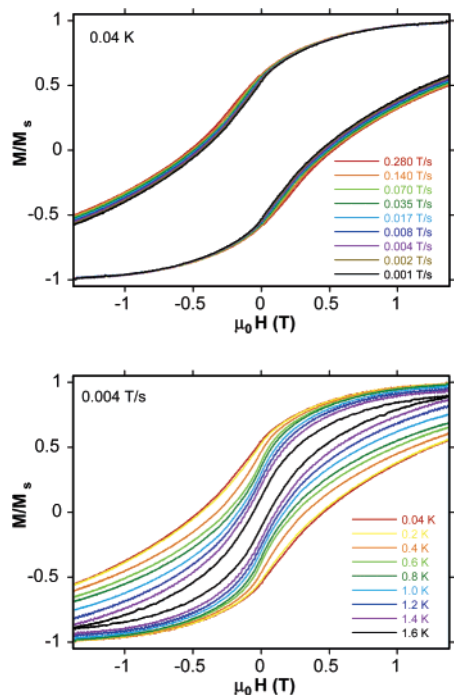


Figure 9. Magnetization (M) vs applied magnetic field hysteresis loops for **2**: (top) in the 0.001–0.280 T/s sweep rate range at 0.04 K; (bottom) in the temperature range 0.04–1.6 K at a 0.004 T/s sweep rate. M is normalized to its saturation value, M_s , for both plots.

temperatures and a fixed field sweep rate are shown in Figures 8 (bottom) and 9 (bottom), respectively. In all cases, hysteresis loops are seen, whose coercivities increase with increasing sweep rate and with decreasing temperature, as expected for the superparamagnet-like properties of a SMM. The data thus confirm complexes **1** and **2** to be new additions to the family of SMMs.

For **1**·8MeOH in Figure 8, the dominating feature in the hysteresis loops is the large step (corresponding to a large increase in magnetization relaxation rate) at zero field due to quantum tunneling of the magnetization (QTM). Steps at other field positions are only poorly resolved, probably due to broadening effects from low-lying excited states and a distribution of molecular environments (and thus a distribution of relaxation barriers) caused by disordered lattice solvent molecules. In addition, intermolecular interactions (both dipolar and exchange) and population of excited states can result in step broadening. Unfortunately, the fast relaxation rate in zero field that results in the large step at this position also prevents us from collecting magnetization vs time decay data with which to construct an Arrhenius plot to determine the effective barrier to relaxation (U_{eff}).

For complex **2**, hysteresis is again evident, but no sign of any steps is observed as a result of broadening effects being more pronounced. Although crystals of **2** do not contain interstitial solvent molecules that can disorder, there is instead extensive disorder in all but one of the carboxylate Bu^t groups seen in the crystal structure, which will have a more significant broadening effect on the magnetic hysteresis by giving a wide distribution of local environments. Again, suitable magnetization vs time decay data could not be obtained for an Arrhenius plot. However, note that a

hysteresis loop is still observed until at least 1.6 K for **2**, even with a slow field sweep rate of 0.04 T/s (the coercivity decreases with decreasing sweep rate). In contrast, the coercivity for **1** is close to disappearing by 1.1 K, even though a faster sweep rate of 0.14 T/s is used (a slower sweep rate was not used to avoid complete collapse of the loop from the fast relaxation at zero field). These data indicate that **2** has a larger barrier to magnetization relaxation than **1**, and this is consistent with the results described above that conclude that **1** and **2** have $S = 5$ and 9 ground states, respectively. This assumes that the D value for the two complexes is comparable (since the barrier is related to $S^2|D|$ for an integer spin system), and this is reasonable given that the Mn^{III} ions in **1** and **2** are the main contributors to the total molecular anisotropy and that both complexes have a similar number of Mn^{III} ions and a similar disposition of their JT elongation axes (since these define the single-ion anisotropy axes and thus their projection onto the total molecular anisotropy). At a qualitative level, therefore, and to some extent at a quantitative level, the various dc and ac data are all consistent.

Finally, note that although we are not reporting the magnetic properties of axially symmetric complex **3** in this paper due to a lack of material, we are submitting elsewhere full details of studies by various techniques on two similarly axially symmetric normal Mn_{12} complexes, those containing $BrCH_2CO_2^-$ or $Bu^tCH_2CO_2^-$ groups. Indeed, preliminary studies on the former have already appeared.^{3k,25}

Conclusions. In this and related work,¹⁵ we have developed a convenient single-source route, via the reductive aggregation of MnO_4^- in MeOH in the presence of carboxylic acid, to a novel family of flat Mn_{12} clusters. Two new members of this family have been reported here, bringing the total number of forms to 3, differing in the number of bridging methoxide (and hydroxide) groups in the core. The structures of **1** and **2** both display two abnormally oriented JT elongation axes. Complexes **1** and **2** are concluded to have $S = 5$ and 9 ground states, respectively. For comparison, we report elsewhere that the third form of these flat Mn_{12} clusters, namely complex **4**, has an $S = 6$ ground state,¹⁵ and it is thus interesting that this structural type can exhibit such different ground-state spin values depending on the exact bridging situation in the central Mn^{IV}_4 core. Hysteresis measurements confirm the addition of **1** and **2** to the growing family of single-molecule magnets (SMMs).

It is clear that the reductive aggregation method has proven its worth as a route to new Mn clusters of various nuclearity and, indeed, as a source of new SMMs. Additional work in this area has provided additional Mn_x species, and these will be reported in due course.

Acknowledgment. We thank the National Science Foundation for support of this work.

Supporting Information Available: X-ray crystallographic data in CIF format for complexes **1**·8MeOH, **2**, and **3**. This material is available free of charge via the Internet at <http://pubs.acs.org>.

IC051150J